JOURNAL OF GEOPHYSICAL RESEARCH, VOL. 94, NO. B12, PAGES 17,383–17,392, DECEMBER 10, 1989

# An Abrupt Change in Ridge Axis Gravity With Spreading Rate

CHRISTOPHER SMALL[1,2] AND DAVID T. SANDWELL[2]

*Institute for Geophysics, University of Texas at Austin*

The global mid-ocean ridge system shows a marked change in morphology and isostatic compensation as a function of spreading rate. Fast spreading ridges have axial highs with little bathymetric relief and low-amplitude gravity signatures indicating that they are nearly in local isostatic equilibrium. Slow spreading ridges have large axial valleys bounded by rugged topography (Macdonald, 1982) and large axial gravity troughs indicating that they are dynamically maintained. While this variation in ridge axis morphology with spreading rate has been observed, it has not been analyzed in a comprehensive manner. Moreover, it is not known whether the transition from axial valley to axial high is a continuous function of spreading rate or whether it occurs abruptly at a particular rate. Such observations would provide important constraints on models of ridge axis dynamics. Vertical deflection profiles collected by the Geosat radar altimeter have sufficient accuracy and resolution to reveal the change in ridge axis gravity with spreading rate. In this study, we have analyzed 44 Geosat profiles over ridges with spreading rates ranging from 14 to 155 mm/yr. In agreement with previous studies, we find that slow spreading ridges (<60 mm/yr) usually have high amplitude gravity troughs (40-100 μrad = 40-100 mGal), while fast spreading ridges (>70 mm/yr) are characterized by low-amplitude ridge axis highs (~15 μrad). Unexpectedly, we find that the transition from axial trough to axial high occurs abruptly at a spreading rate of 60-70 mm/yr. Ridge axis gravity signatures are highly variable for rates less than 65 mm/yr and very uniform at higher rates. The transition of the gravity signature appears to be more abrupt than the transition of the topographic signature, suggesting an abrupt change in the style of isostatic compensation with spreading rate. Published models of ridge axis dynamics do not explain this sharp transition.

## INTRODUCTION

The topography of the mid-oceanic ridge system shows a systematic variation with spreading rate [*Menard*, 1967; *Macdonald*, 1986]. This has been shown extensively on the East Pacific Rise and Mid-Atlantic Ridge (Project RISE, Project FAMOUS). At slower spreading rates (10-50 mm/yr full rate) the topography is rugged and is dominated by a deep (1.5-3.0 km) axial rift valley [*Macdonald and Luyendyk*, 1977]. At intermediate rates (50-90 mm/yr) the topography is smoother and the axial valley is less pronounced (50-200 m) [*Klitgord and Mudie*, 1974]. At fast spreading rates (>90 mm/yr) the axial valley disappears and is replaced by a narrow axial ridge [*Rea*, 1978]. In addition to spreading rate, axial valley depth depends upon distance to the nearest transform fault as well as proximity to a hot spot [*Macdonald*, 1986]. Because of these additional factors, the transition from axial valley to axial high is a gradual function of spreading rate.

Several theoretical models have been proposed to explain this variation in spreading ridge morphology. Most models involve a weak fluid overlain by an elastic plate. *Sleep* [1969] proposed a model in which the lithosphere cools to form a conduit through which molten asthenosphere is supplied to form oceanic crust. The axial valley is considered to be the result of a hydrostatic pressure drop or "loss of head" in the conduit. *Tapponier and Francheteau* [1978] have proposed that the axial valley is a result of steady state necking of the oceanic lithosphere at the accreting plate boundary. Inherent in both of these models are assumptions concerning the dimensions (or existence) of the magma chamber which supplies the ridge as well as the thickness of the plates at the ridge axis. *Phipps Morgan et al.* [1987] have provided a detailed analysis of several mechanisms for the formation of oceanic crust. Their favored model invokes horizontal extensional stresses to produce internal bending moments and flexure of a perfectly plastic plate. All of the models considered above have advantages and drawbacks as a result of various assumptions and simplifications. The actual ridge axis involves complex thermal, mechanical, and chemical interactions such as the interaction of viscous melt rheology and cooling due to hydrothermal circulation. Because of these complications it is not well understood how the topography is controlled by the extensive faulting in the axial valleys. One particularly intriguing problem is the mechanism by which the two radically different tectonic environments are related. Relatively little attention has been given to the physical transition from one end-member to the other.

Gravity surveys on ridges of different spreading rates have provided useful constraints on the processes responsible for creation of oceanic crust. To determine the effective elastic thickness (EET) of the lithosphere at ridge axes, *Cochran* [1979] analyzed the relationship between gravity and bathymetry on the Mid-Atlantic Ridge and on the East Pacific Rise. He found that slow spreading ridges have EETs ranging from 7 to 13 km, while fast spreading ridges have lower EETs ranging from 2 to 6 km. This difference in plate thickness is related to ridge axis temperatures and may be responsible for the change in ridge axis morphology with spreading rate. *Collette et al.* [1980] carried out a detailed analysis of the gravity and topography the Mid-Atlantic Ridge axis. They modeled the spreading ridge axis as a viscous sheet undergoing continuous unloading and found that the depth of the median valley depends primarily on the viscosity of the sheet; a fast spreading ridge should be hotter and have a less viscous sheet than a slow spreading ridge. Moreover, they suggested that the Reykjanes Ridge does not have an axial valley because low-viscosity material is upwelling above the Iceland hot spot.

More recently, *Chen and Morgan* [1987] proposed a single model to explain the morphologies of both slow and fast spreading ridges. Beneath slow spreading ridges, the crust is relatively cool and remains brittle. The brittle crust deforms plastically and is strongly

[1]also at Department of Geological Sciences, University of Texas at Austin.

[2]Now at Geological Research Division, Scripps Institution of Oceanography, La Jolla, California.



Paper number 89JB01082.
0148-0227/89/89JB-01082$05.00

coupled to the mantle so a rift valley develops. As the spreading rate is increased, however, a weak ductile zone develops just above the Moho. If the width of the ductile zone exceeds the width of the plastically deforming zone, then the crust becomes decoupled from the mantle. When this occurs, the ridge axis can rebound to local isostatic equilibrium resulting in a central high. The model predicts that the transition from axial valley to axial high will occur abruptly at a particular spreading rate (~76 mm/yr).

In order to determine the variation in ridge axis structure and dynamics with spreading rate, a detailed analysis of the global spreading ridge system is needed. The end-members of the system, particularly the Mid-Atlantic Ridge and East Pacific Rise, have been studied extensively and compared, but a comprehensive investigation of the entire spreading ridge system has yet to be undertaken. Most notably, the ridge systems in the southern oceans have been neglected despite the fact that they comprise almost half of the total length of the worlds spreading ridge system. Since a single, uniform, global study would be very costly using conventional geophysical survey methods, it is necessary to use an alternative technique.

Here we present a systematic analysis of the global spreading ridge system using vertical deflection (gravity) profiles derived from Geosat satellite altimeter data. The vertical deflection is the slope of the equipotential sea surface and is a direct measure of the horizontal component of the gravity anomaly vector (1 mGal = 0.98 μrad). Using highly accurate (<2 μrad) Geosat repeat profiles, we have performed a global analysis of vertical deflection signatures over 44 ridge axis segments with full spreading rates ranging from 14 to 155 mm/yr. The uniform coverage and consistent treatment of the data make it possible to evaluate objectively the entire spectrum of full spreading rates and ridge axis gravity signatures.

The vertical deflection (gravity) signature of a ridge axis depends primarily upon two factors, the topography of the seafloor and the degree and style of isostatic compensation. It is important to remember that we are studying vertical deflection and not topography. Although seafloor topography has a primary influence on short-wavelength vertical deflection, there are differences. The fine scale topography of the ridge axis (wavelength <2π x ocean depth or ~15 km) is attenuated in sea surface gravity measurements. Moreover, at the longer wavelengths (>2π x Moho depth or ~60 km), isostatic compensation can significantly reduce the gravitational influence of the topography. Thus our ridge axis gravity results cannot be directly compared with the ridge axis topography results of *Macdonald* [1986]; the combination of the two data types may improve our understanding of ridge axis dynamics.

Schematic diagrams of the topography, geoid height, and vertical deflection signatures across slow spreading and fast spreading ridge axes are shown in Figure 1. Slow spreading ridges (Figure 1*a*) have relatively steep flanks due to the increase in seafloor depth with age and the rapid increase in age with distance away from the ridge. The ridge axis is characterized by a deep central trough and flank uplifts. The geoid profile roughly mimics the topography although it decreases linearly with age away from the ridge rather than as the square root of age [*Haxby and Turcotte*, 1978]. The vertical deflection is the along-track derivative of the geoid profile. Thus it is positive on the ridge flank approaching the axis and negative on the far flank. Above the axis the vertical deflection is first negative going into the trough and then positive coming out of the trough; the inflection point marks the spreading axis.

The characteristics of fast spreading ridges are quite different (Figure 1*b*). Because of the high spreading rate, the ridge flank gradient is low. Moreover, the ridge axis is a small narrow peak instead of a deep wide trough. The geoid profile mimics the topography, so the geoid height variations are also small. The vertical deflection profile is only slightly positive on the ridge flank approaching the axis and slightly negative on the far side. In contrast to the slow spreading ridge, the ridge axis signature is a peak followed by a trough instead of a trough followed by a peak. The overall vertical deflection signature is narrow (~10 km) and has a low amplitude (~15 μrad). Such a short-wavelength, low-amplitude signal is below the resolution capabilities of Seasat altimeter profiles or even individual Geosat profiles. To increase the short-wavelength signal to noise ratio, we averaged 22 repeat Geosat profiles.

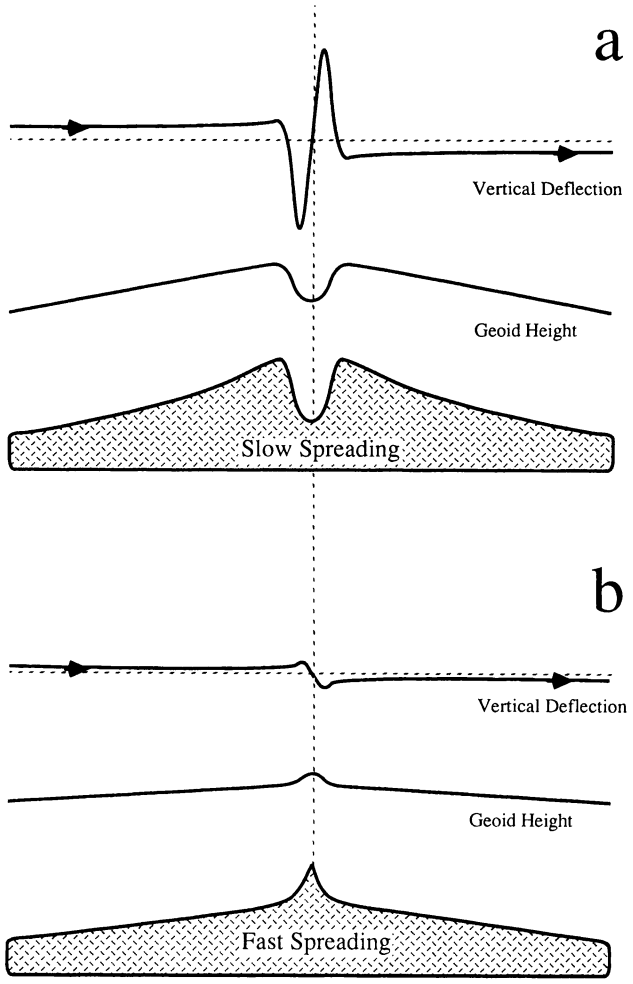


**Fig. 1. Schematic diagram showing the differences in the geoid (sea surface) and the corresponding vertical deflection for fast and slow spreading ridges. (*a*) A slow spreading ridge has an axial valley and significant relief on the ridge flanks. The geoid height shows the axial valley and a linear decrease away from the axis. The vertical deflection (along the satellite ground track) has a large amplitude trough followed by a peak. (*b*) A fast spreading ridge has an axial high and little axial relief near the ridge. The geoid height shows only a small bump. The vertical deflection has reversed polarity with a peak followed by a trough.**

## DATA ANALYSIS

A complete description of the Geosat mission may be found in the *Applied Physics Laboratory* [1987] (APL) *Technical Digest*. Our processing of the data was designed to enhance the short-wavelength, low-amplitude gravity variations associated with spreading ridges. First, Geosat geophysical data records [*Cheney et al.*, 1987] were edited when the rms of the 1-s averages exceeded 0.15 m. The data were then compressed from 10 points/s to 2 points/s by averag-

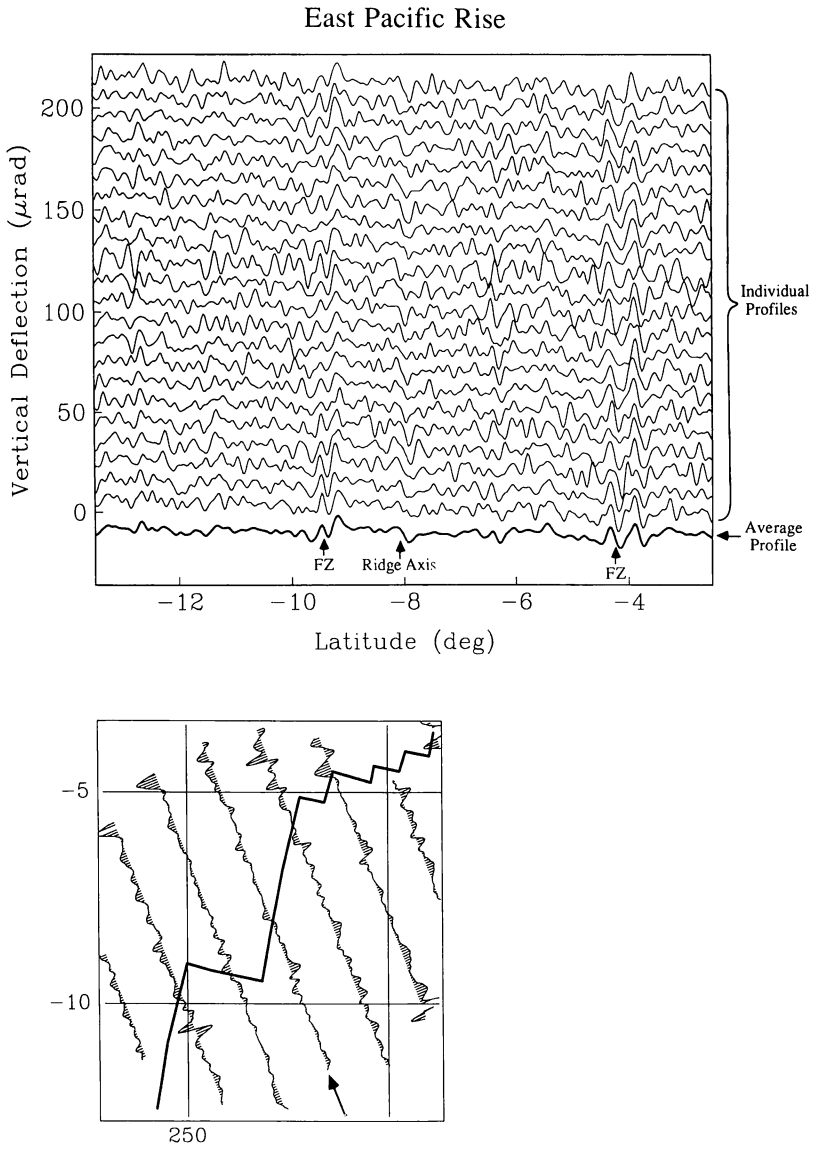


**Fig. 2. Averaging many (22) repeat cycles improves the accuracy and resolution of the Geosat altimeter data (top). Vertical deflection profiles across the fast spreading East Pacific Rise have very low amplitude anomalies associated with the ridge axis and fracture zones (FZ). These small anomalies are not resolved in individual Geosat profiles.**

ing five adjacent points resulting in an along-track spacing of 3.4 km. To enhance the short-wavelength features in the marine geoid, Geosat profiles were differentiated along track using the first difference formula. This derivative also suppresses the longer-wavelength radial orbit error and the path length errors. Along-track deflections of the vertical, in microradians, were obtained by dividing the time derivative of each pass by the along-track velocity of the satellite. To remove the shortest-wavelength noise, which is amplified by differentiation, each pass was low-pass filtered using a Gaussian filter with a cutoff wavelength of ~15 km ( $\exp[-x^2/2\sigma^2]$, $\sigma$ = 5.7 km).

The most important step in the data processing was to average 22 Geosat repeat cycles in order to reduce the altimeter noise. This was done by interpolating and registering the individual repeat cycles and then averaging them together. An example of the individual Geosat repeat profiles and the average profile across the East Pacific Rise is shown in Figure 2. This ascending track exhibits the characteristic peak to trough signature where it crosses the East Pacific Rise at -8° latitude. Note that the individual profiles do not have a clear expression of the ridge axis because altimeter noise dominates the low-amplitude signal. After averaging, the altimeter noise is reduced to 2 μrad or less so that the lowest amplitude ridge axis signatures (~15 μrad) are apparent.

The final step in the processing was to remove the long-wavelength (>4000 km) variations in the vertical deflection using the PGS-S4 gravity model [*Marsh and Martin*, 1982] to degree and order 36. The spherical harmonic coefficients were tapered at degree 10 to reduce the side lobes caused by truncation.

For the analysis of the global spreading axis, we selected 44 locations on the basis of spreading rate, spatial distribution and distance from fracture zones (Figure 3 and Table 1). The 44 areas provide a uniform distribution of spreading velocities between 14 and 155 mm/yr. Also included are data from some acknowledged anomalous ridges (Reykjanes, Cocos, Australian-Antarctic Discordant Zone). Spreading rates were calculated using the NUVEL-1 current plate motion model of R. G. Gordon et al. (personal communication, 1988). All velocities given are full spreading rates. The spatial distribution of points covers every major spreading center but

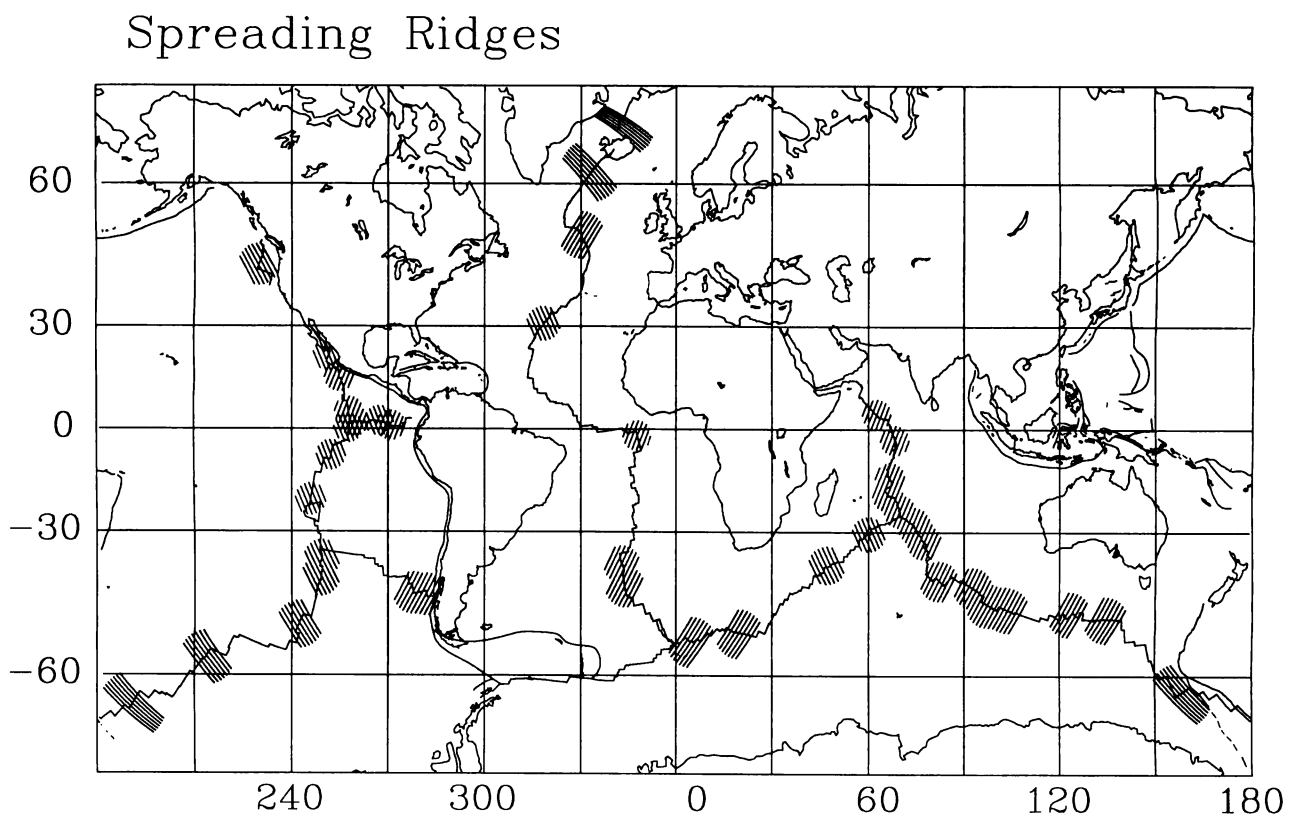


Fig. 3. The global distribution of spreading ridges used in this study. One representative track was selected from each of the 44 regions. The high density of fracture zones and the orientation of the satellite ground tracks eliminated most of the Mid-Atlantic Ridge between -30° and +30°.

is constrained by the presence of fracture zones and the orientation of the satellite's ground track.

The global spreading ridge axes used to select and analyze the profiles were from a data base compiled by *Gahagan et al.* [1988]. Ridges and transform boundaries were picked according to the General Bathymetric Chart of the Oceans (GEBCO) [*Canadian Hydrographic Service*, 1982] as well as from other published bathymetric charts. In areas of sparse bathymetric coverage, earthquake epicenters and Seasat altimeter profiles were used to define the plate boundary. We found several areas where the location of the ridge in the data base was offset from the apparent ridge location as shown in the Geosat data. In these areas we used the Geosat data to define the ridge axis.

Only those passes which cross the ridge axis at an angle greater than 25° were considered. Since the Geosat ground track is composed of ascending and descending passes, this did not pose a serious problem in itself, but coupled with the constraint imposed by fracture zones, it did eliminate several ridge segments from consideration. Fracture zones have prominent geoid signatures with amplitudes that are typically greater than the adjacent ridge axis signatures. In addition, it is well known that axial valleys are often present adjacent to ridge-transform intersections [*Macdonald*, 1986]. For these reasons, we used only ridge segments more than ~50 km from prominent fracture zones. This imposed the greatest constraint along the Mid-Atlantic Ridge where there is a high density of fracture zones. In each of the 44 areas we initially selected all of the data within a 500-km radius of a point centered on the longest ridge segment. From each data set we then selected the pass which best satisfied all of the criteria mentioned above.

The 44 best profiles were projected perpendicular to the ridge by multiplying the along-track distance from the crossing point by the cosine of the angle of intersection. Since the vertical deflection is the derivative of the geoid height with respect to the along-track distance, it was also necessary to divide its amplitude by the cosine of the angle. From the projected profiles we measured the peak to trough amplitude of the ridge axis signature its width and its polarity. Four projected profiles are shown in Figure 4. As the altimeter passes over a ridge with an axial high (i.e., upper two profiles in Figure 4), the deflection of the vertical has a peak followed by a trough (positive polarity). As the altimeter passes over a ridge with an axial valley (i.e., lower two profiles in Figure 4), the deflection of the vertical has a trough followed by a peak (negative polarity).

While the measurements of the peak to trough amplitude and polarity of the vertical deflection signature are straightforward, a couple of problems can arise because of errors in the plate boundary and uncharted fracture zones. First, the polarity can be reversed if the ridge-axis (i.e., 0 offset in Figure 4) is mislocated by more than about 15 km. In the few cases we chose the ridge axis location using the Geosat profiles. In these cases, our chosen polarities may be biased toward the polarity that we expected (see below). While this problem affects the polarity measurements, it does not affect the amplitude measurements which are insensitive to the location of the axis. The second problem occurs when measuring the peak to trough amplitude along profiles where there are uncharted fracture zones causing unrelated peak and trough signatures. This problem occurred mainly along slow spreading ridges where the fracture zones are closely spaced.

## RESULTS

Vertical deflection profiles over all 44 ridge axes are presented in Figure 5 in order of increasing spreading rate. Most of the slower spreading ridges (<60 mm/yr) have signatures similar to the sche

TABLE 1. Ridge Axis Data

| Ridge | Latitude deg | Longitude deg | Plate #[a] From | To | Spreading Rate mm/yr | Average Axis Depth km | Ascending Descending | Peak to Trough μrad |
|---|---|---|---|---|---|---|---|---|
| SW Indian | -54.3 | 4.9 | 1 | 2 | 13.9 | 1.9 | D | -78.5 |
| SW Indian | -52.8 | 19.8 | 1 | 2 | 14.4 | 2.6 | D | -107.1 |
| SW Indian | -30.5 | 60.0 | 1 | 2 | 14.5 | 2.2 | A | -104.9 |
| SW Indian | -38.3 | 47.0 | 1 | 2 | 14.8 | 1.8 | A | -81.8 |
| Reykjanes | 68.2 | 341.8 | 6 | 10 | 18.5 | 0.5 | A | 17.4 |
| Reykjanes | 61.6 | 332.9 | 6 | 10 | 20.4 | 1.0 | A | 40.6 |
| Mid-Atlantic | 51.0 | 330.0 | 6 | 10 | 22.7 | 2.3 | D | -79.9 |
| Mid-Atlantic | 30.7 | 318.2 | 1 | 10 | 23.5 | 2.4 | A | -80.2 |
| Central Indian | 4.5 | 62.5 | 1 | 7 | 29.4 | 2.7 | D | -33.5 |
| Mid-Atlantic | -2.0 | 347.5 | 1 | 12 | 33.3 | 2.7 | D | -114.6 |
| Mid-Atlantic | -43.3 | 343.8 | 1 | 12 | 34.3 | 2.3 | D | -66.5 |
| Central Indian | -3.4 | 68.2 | 1 | 7 | 35.0 | 2.8 | D | -56.6 |
| Mid-Atlantic | -38.2 | 342.8 | 1 | 12 | 35.2 | 2.2 | D | -85.3 |
| Central Indian | -14.8 | 66.7 | 1 | 8 | 38.8 | 2.4 | D | -81.6 |
| Cocos | 2.2 | 259.2 | 5 | 9 | 42.2 | 2.7 | D | -26.0 |
| Central Indian | -19.8 | 66.0 | 1 | 8 | 43.1 | 2.5 | D | -31.2 |
| Central Indian | -24.3 | 69.8 | 1 | 8 | 48.7 | 2.7 | D | -34.0 |
| Cocos | 2.4 | 267.2 | 5 | 9 | 55.2 | 2.4 | A | 23.5 |
| Juan de Fuca | 44.9 | 229.7 | 11 | 13 | 59.6[b] | 2.5 | A | 25.9 |
| Chile Rise | -44.7 | 277.9 | 2 | 9 | 60.4 | 3.0 | D | -59.5 |
| Chile Rise | -45.0 | 282.0 | 2 | 9 | 60.5 | 2.7 | D | -38.3 |
| SE Indian | -27.8 | 74.0 | 2 | 8 | 60.8 | 2.8 | D | -42.2 |
| Cocos | 1.0 | 270.8 | 5 | 9 | 60.9 | 2.2 | D | 22.6 |
| Pacific Antarctic | -64.1 | 191.0 | 2 | 11 | 61.4 | 2.6 | A | 10.5 |
| SE Indian | -29.0 | 74.9 | 2 | 8 | 61.8 | 2.7 | D | -40.0 |
| E Pacific | 22.0 | 251.4 | 11 | 14 | 62.0[c] | 2.6 | A | 11.6 |
| SE Indian | -32.5 | 77.5 | 2 | 8 | 64.7 | 2.6 | D | -9.7 |
| SE Indian | -62.4 | 158.0 | 2 | 8 | 68.3 | 2.5 | A | 20.9 |
| SE Indian | -42.0 | 82.1 | 2 | 8 | 70.1 | 2.7 | D | 9.8 |
| SE Indian | -43.5 | 92.7 | 2 | 8 | 73.0 | 2.7 | D | 15.8 |
| SE Indian | -50.1 | 134.5 | 2 | 8 | 73.2 | 2.8 | D | 16.1 |
| SE Indian | -47.2 | 97.3 | 2 | 8 | 74.3 | 2.7 | D | 11.4 |
| SE Indian | -47.9 | 102.5 | 2 | 8 | 74.9 | 3.0 | D | -12.7 |
| SE Indian | -49.7 | 121.6 | 2 | 8 | 75.0 | 3.4 | D | -39.0 |
| SE Indian | -48.2 | 103.8 | 2 | 8 | 75.1 | 3.0 | D | 24.4 |
| Pacific Antarctic | -57.0 | 213.9 | 2 | 11 | 77.2 | 2.6 | A | 12.2 |
| E Pacific | 15.9 | 254.7 | 5 | 11 | 83.7 | 2.8 | D | 14.5 |
| Pacific Antarctic | -51.1 | 242.4 | 2 | 11 | 89.0 | 2.7 | A | 8.9 |
| Pacific Antarctic | -41.0 | 249.0 | 2 | 11 | 96.5 | 2.7 | A | 13.8 |
| Pacific Antarctic | -36.8 | 249.4 | 2 | 11 | 98.4 | 2.7 | A | 12.2 |
| E Pacific | 5.2 | 257.7 | 5 | 11 | 123.6 | 2.9 | D | 17.3 |
| E Pacific | 0.3 | 257.5 | 9 | 11 | 131.4 | 2.9 | A | 8.2 |
| E Pacific | -8.0 | 252.1 | 9 | 11 | 143.7 | 2.8 | A | 14.2 |
| E Pacific | -21.1 | 245.9 | 9 | 11 | 155.4 | 2.8 | A | 5.5 |

The ridges are given in order of increasing spreading velocity. The velocities are given in full rates and are obtained from the NUVEL-1 model of R.G. Gordon et al. (manuscript in preparation, 1988). Average ridge axis depths are from *Anderson et al.* [1973].

[a]Plate names: 1, African; 2, Antarctic; 3, Arabian; 4, Caribbean; 5, Cocos; 6, European; 7, Indian; 8, Australian; 9, Nazca; 10, North American; 11, Pacific; 12, South American; 13, Juan de Fuca; 14, Rivera.

[b]Spreading rate from *Hey and Wilson* [1982].

[c]Spreading rate from *Klitgord and Mammerickx* [1982].

matic profile shown in Figure 1*a*. For example, the descending profiles across the Southwest Indian Ridge (area 2, 14.4 mm/yr) are positive approaching the ridge axis from the north, and negative on the south side of the ridge axis. These characteristics are in accordance with the cooling and subsidence of the oceanic lithosphere with age [*Haxby and Turcotte*, 1978]. Directly above the ridge axis, the vertical deflection profiles have large amplitude troughs followed by peaks (~-100 μrad peak to trough). While there is only one published bathymetric profile across this 500-km-long segment of the ridge axis, we believe the trough to peak signature is due to a deep axial valley.

A major change in the ridge axis gravity signature occurs when the spreading rate exceeds about 65 mm/yr (area 28 in Figure 5). At these higher rates, the vertical deflection profiles have the distinct characteristics of the fast spreading ridge (Figure 1*b*). For example, the descending profiles across the Southeast Indian Ridge (area 30 spreading at 73.0 mm/yr) are slightly positive approaching the ridge axis from the north and slightly negative on the south side. The ridge axis signature is a low amplitude, short wavelength peak followed by a trough (~15 μrad peak to trough) that we believe is caused by a small axial high in the topography.

From an examination of the data shown in Figure 5, it is evident that there is an major change in the nature of ridge axis gravity anomalies (and abyssal hills and fracture zones) that occurs at a rate of 60-70 mm/yr. Below this rate, the ridge axis gravity signature has high amplitudes and is variable. Above this rate, the ridge axis gravity signature has low amplitudes and is uniform. (All of the data are plotted at the same scale of 30 μrad per degree of longitude.)

As described in the data analysis section, we chose one profile from each of the 44 areas and measured the peak to trough amplitude

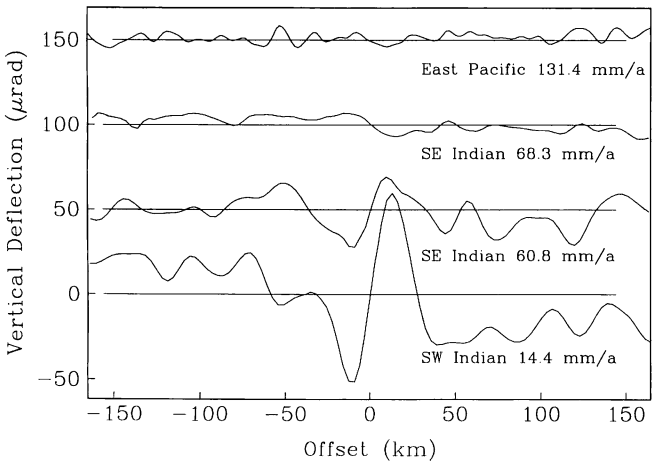


Fig. 4. Examples of projected profiles at four significant spreading rates. The lower two profiles over slow spreading ridges have a trough before a peak and a large amplitude signal at the ridge axis. The upper two profiles over fast ridges have a smaller amplitude signature and a peak before a trough. Note the change in signature between 60.8 and 68.3 mm/yr.

and width of the ridge-axis gravity signature. The results are summarized in Table 1 where the name, location, plate number, full spreading rate (R. G. Gordon et al., personal communication, 1988), average ridge axis depth [*Anderson et al.*, 1973], and peak to trough vertical deflection amplitudes are also listed. Slow spreading ridges (<60-65 mm/yr) usually have high amplitude trough to peak signatures (40-100 μrad = 40-100 mGal) while fast spreading ridges (>65-70 mm/yr) are characterized by low amplitude peak to trough signatures (~15 μrad). There are several exceptions to this general rule, however. First, the Reykjanes Ridge is spreading at a very low rate (~20 mm/yr) yet it has the low-amplitude and positive, peak to trough gravity expression that is characteristic of a fast spreading ridge. Second, the Southeast Indian Ridge between longitudes of 100° and 128° is spreading at rate that is slightly higher than the proposed transition rate (~75 mm/yr) yet it has a negative peak to trough gravity signature that is characteristic of a slow spreading ridge; along the Australian-Antarctic Discordant Zone the peak to trough expression is quite low (-40 μrad). In addition to having anomalous gravity signatures, these ridges are anomalously shallow and deep, respectively.

To further illustrate the anomalous ridges, we have plotted the

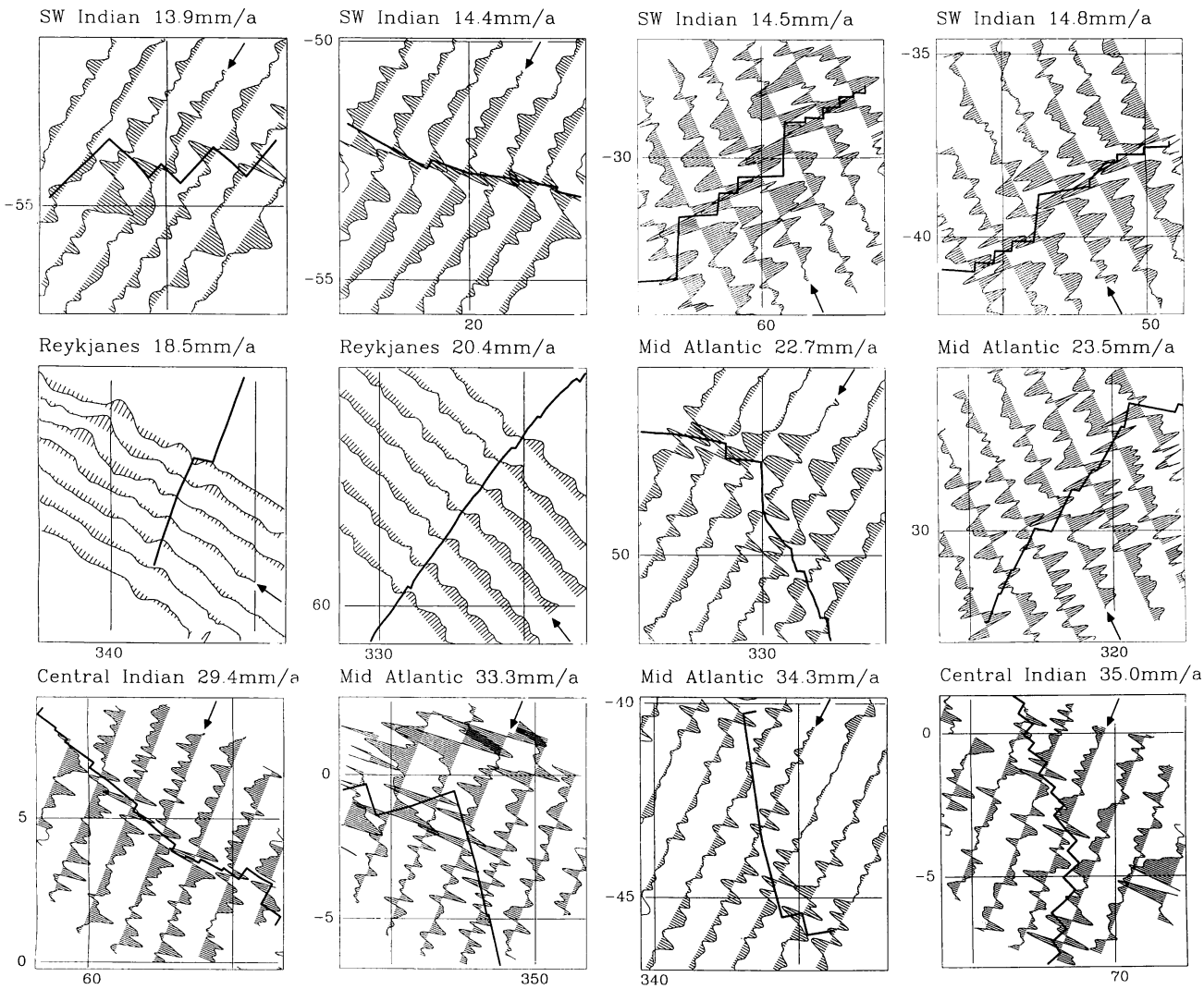


Fig. 5. Along-track vertical deflection profiles across 30 spreading ridges. An anomaly of 30 μrad spans 1° of longitude. The slow spreading ridges (<65 mm/yr) have usually large amplitude troughs followed by peaks, while the fast spreading ridges (>65 mm/yr) have small-amplitude peaks followed by troughs. Ascending profiles run southeast to northwest while descending profiles run northeast to southwest.

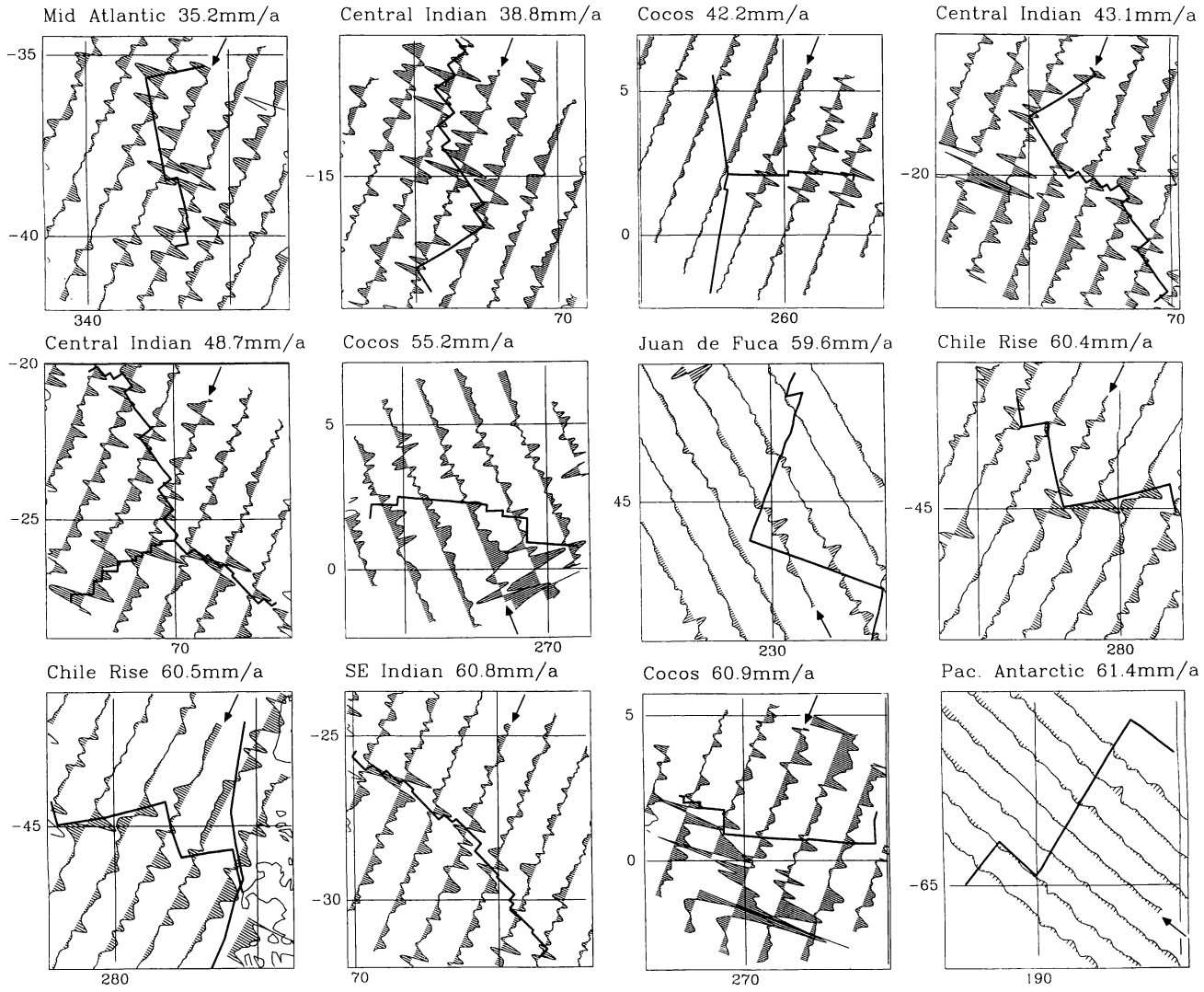


Fig. 5. (continued)

peak to trough ridge amplitude versus the average ridge crest depth for each of the 44 ridges (Figure 6). Ridge crest depths were taken from *Anderson et al.* [1973] except for the Juan de Fuca Ridge and the Chile Rise where depths were taken from the GEBCO charts [*Canadian Hydrographic Service*, 1982]. The global average ridge crest depth is 2503 ± 442 m [*Anderson et al.*, 1973]. We consider that ridges that are more than one standard deviation from the mean depth are anomalous. For our 44 areas, most ridge crests have depths between 2 and 2.9 km; only 8 of our 44 examples fall outside of this range. The points that are too shallow lie on the Reykjanes and SW Indian ridges while the points that are too deep lie on the Southeast Indian Ridge and the Chile Rise. As discussed below, the ridges with anomalous gravity signatures are also anomalously shallow or deep. This suggests that there is a secondary relationship between ridge crest depth and ridge axis gravity.

The primary correlation is between ridge axis gravity and spreading rate as shown in Figure 7. (Triangles, squares, and circles indicate the general location of the data point, Atlantic, Pacific, or Indian Ocean.) As in Figure 6, solid symbols represent ridges having average depths between 2 and 3 km, while the deeper and shallower ridges are represented by open circles. If these "anomalous ridges" are disregarded, then ridge axis gravity versus spreading rate can be characterized by two lines having an abrupt change in slope at 65 mm/yr (dashed lines in Figure 7). Between spreading rates of 15 and 65 mm/yr, the characteristic peak to trough gravity signature increases from -120 to 15 μrad. In contrast, between 65 and 155 mm/yr there is a gentle decline in peak to trough gravity from 15 to 10 μrad. The change in polarity between axial valley and axial high occurs at a rate of ~60 mm/yr. In addition to these changes in polarity and slope, there is a marked change in the scatter about the two lines. For rates less than 65 mm/yr the data are highly scattered about the linear trend model, while for rates greater than 65 mm/yr the data are well fit by a linear trend with near zero slope.

## DISCUSSION

From this analysis we conclude that the vertical deflection signature of the global spreading ridge system shows an abrupt change in character that occurs at a full spreading rate of ~60-70 mm/yr (Figure 7). As the spreading rate increases, the change in the vertical deflection signature is threefold; a decrease in amplitude, a change in polarity, and a decrease in the degree of variability. These findings are consistent with the bathymetric observations of [*Menard*, 1967; *Macdonald*, 1982] although the distinction between intermediate and fast spreading ridges pointed out by *Macdonald* [1982] is not apparent in the vertical deflection data; the change in the ridge axis gravity signature is more abrupt than the corresponding change in the ridge axis topography signature. Since gravity depends upon both

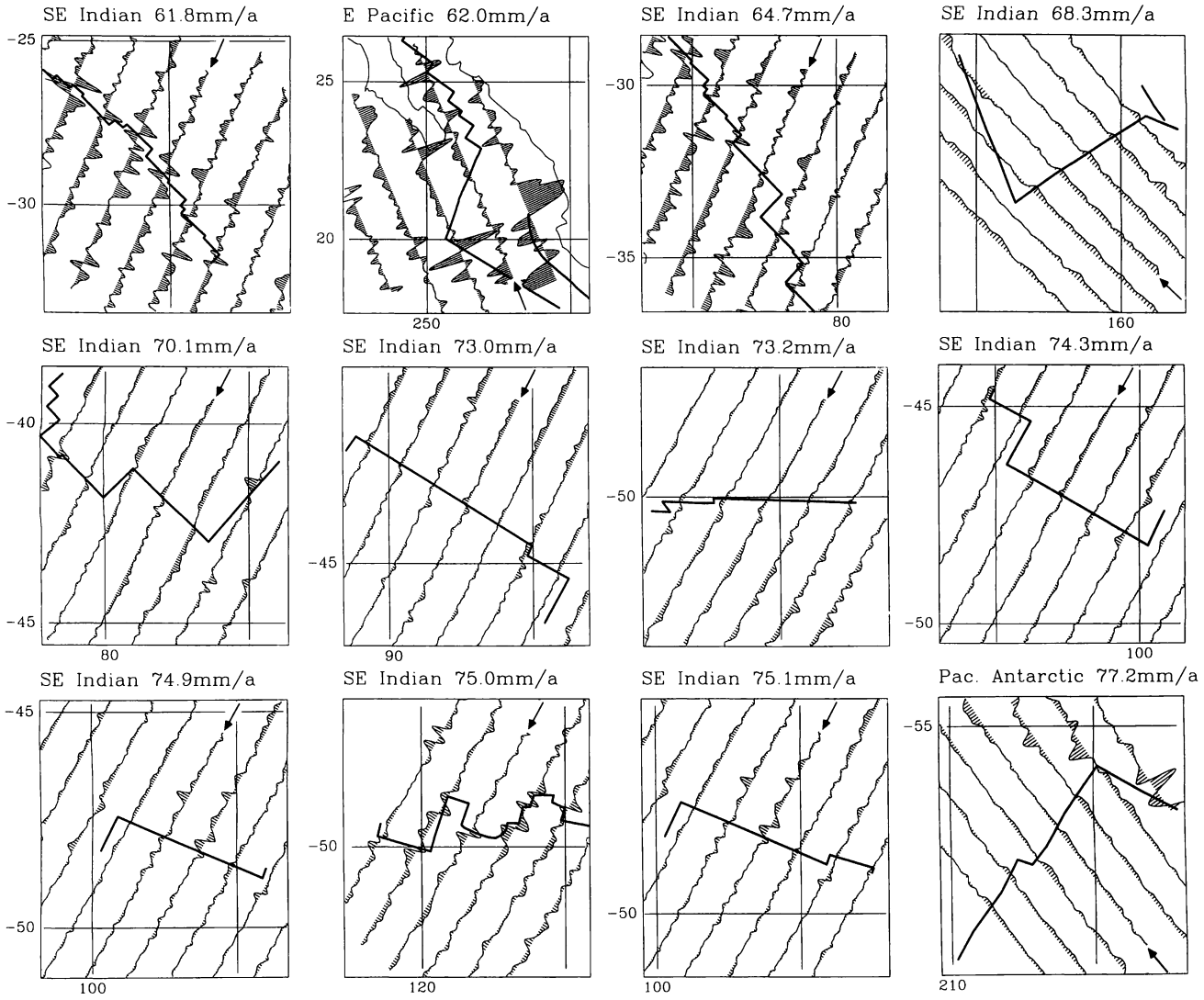


Fig. 5. (continued)

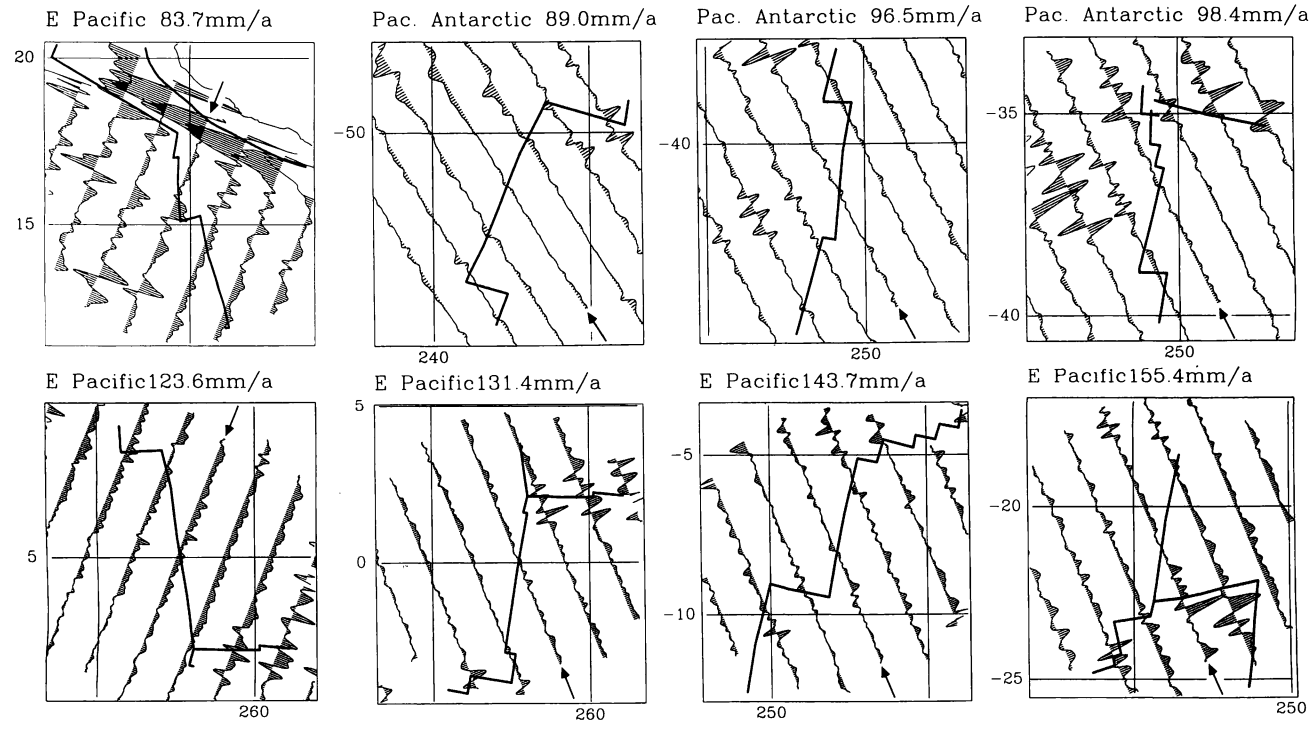


Fig. 5. (continued)

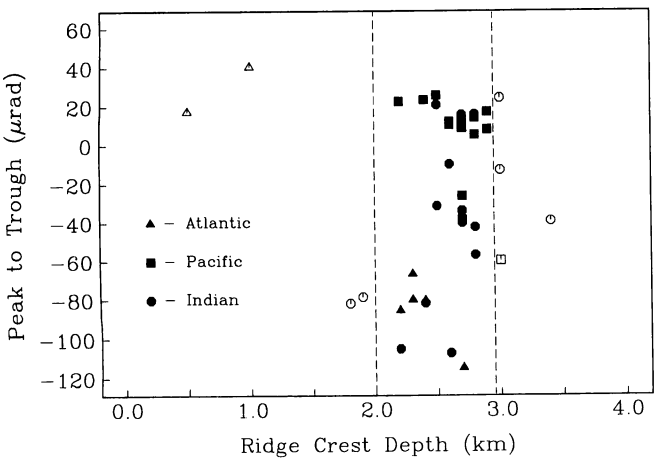


Fig. 6. Peak to trough vertical deflection over 44 ridge axes versus the average axial depth of the ridge. Triangles, Mid-Atlantic Ridge; squares, Juan de Fuca, East Pacific Rise, Cocos, Chile, and Pacific-Antarctic ridges; circles, Central Indian, Southwest Indian, and Southeast Indian ridges. Most ridge crests have depths between 2 and 3 km (solid symbols). Four ridges are shallower than 2 km and four are deeper than 2.9 km (open symbols). Peak to trough amplitude and ridge crest depth are only weakly correlated.

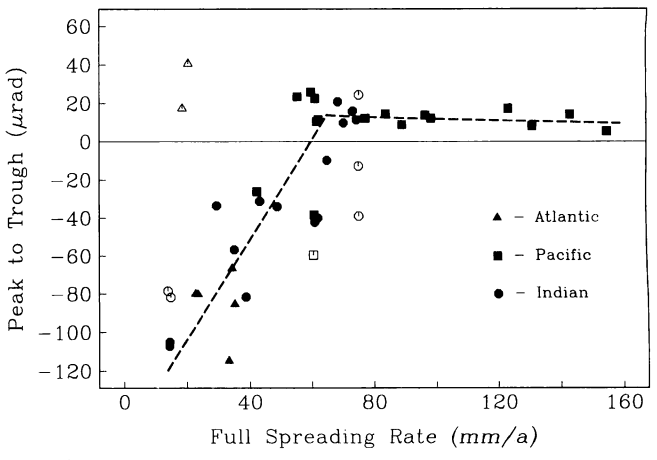


Fig. 7. Peak to trough vertical deflection over 44 ridge axes versus full spreading rate. Symbol shape indicates major ocean. Open symbols are "anomalous" ridges that are either shallower than 2 km or deeper than 2.9 km (see Figure 5). Peak to trough amplitudes are usually negative and highly variable for rates less than 65 mm/yr while at higher rates, amplitudes are positive and uniform. Dashed lines have an abrupt change in slope at 65 mm/yr.

the topography and the compensation mechanism, the abrupt change in the gravity signature must signify an abrupt change in the compensation mechanism. The implication is that there are two dynamically distinct modes of seafloor spreading.

The high amplitude and high variability of the ridge axis gravity along slow spreading ridges (Figure 7, <65 mm/yr) may result from a complicated interaction of hydrothermal cooling, brittle fracturing and ductile necking of highly non uniform material. As pointed out by *Macdonald* [1982], the variability in ridge axis morphology could be caused by episodic spreading. However, it could also be explained by necking and brittle fracture of the crust. For that matter, it is reasonable to believe that the process of necking and brittle fracture of the crust may be a highly episodic phenomenon rather than a smooth continuous process. In any case, the high amplitude and variability, of slow spreading ridge axes, are apparent in both the bathymetric and the gravity observations.

The low amplitude and low variability in vertical deflection for fast spreading ridges (Figure 7, >65 mm/yr) indicate that mid-oceanic ridge topography is well compensated and is relatively uniform. (Along-strike variations occur along fast spreading ridges, but their amplitudes are small compared with the slow spreading ridges.) The relatively uniform gravity could either be due to uniform spreading or may simply indicate that the ridge axis is nearly in local isostatic equilibrium.

The only significant departures from the general trend of the data (Figure 7) are the polarities of the two samples from the Reykjanes Ridge and the two samples from the Australian-Antarctic Discordant Zone. As shown above, and in previous studies, these ridges are anomalously shallow and deep, respectively. As proposed by *Vogt* [1976], upwellings and downwellings in the mantle beneath ridge axes may influence both ridge axis depth and morphology. However, we believe that these local variations in mantle flow and temperature have only a secondary effect on the morphology of the ridge axis and its compensation mechanism; the primary influence is spreading rate.

Except for the unpublished model of *Chen and Morgan* [1987], no ridge crest models predict such an abrupt change in morphology and compensation mechanism with increasing spreading rate. A brief comparison of the gravity data in Figure 5 clearly indicates that there is a significant change in the nature of ridge crests at fast and slow spreading rates. In addition to the abrupt change in the signature of the ridge itself, there is also a decrease in the density of fracture zones and abyssal hills with increasing spreading rate. This suggests that the change from slow to fast spreading is a discontinuous process that may be considerably more complicated than previously believed.

*Acknowledgments.* We wish to thank Jan Garmany, Cliff Frohlich, and the members of the Spring 1988 Geodynamics class at the University of Texas at Austin for helpful comments and suggestions. We also wish to thank Yongshun Chen, Ken Macdonald, and the Associate Editor for constructive criticism of the initial draft. This research was supported by the NASA Geodynamics Program (NAG 5-787) and the Texas Advanced Technology Research Program.

## REFERENCES

Anderson, R. R., D. P. McKenzie, and J. G. Sclater, Gravity, bathymetry and convection in the Earth, *Earth Planet. Sci. Lett., 18*, 391-407, 1973.

Applied Physics Laboratory, *Johns Hopkins APL Tech. Dig., 8*(2), Laurel, Md., 1987.

Canadian Hydrographic Service, *General Bathymetric Chart of the Oceans (GEBCO)*, 5th ed., Ottawa, Ont., 1982.

Chen, Y.J., and W. J. Morgan, A mechanical model for the contrast between the broad rift valleys on slow spreading centers and no valleys on fast spreading ones, *Eos Trans. AGU, 68*,(16), 407, 1987.

Cheney, R.E., B.C. Douglas, R.W. Agreen, L. Miller, D.L. Porter, and N.S. Doyle, Geosat altimeter geophysical data record user handbook, *NOAA Tech. Memo. NOS NGS-46*, 1987.

Cochran, J.R., An analysis of isostasy in the world's oceans, 2, Mid-ocean ridge crests, *J. Geophys. Res., 84*, 4713-4729, 1979.

Collette, B.J., J. Verhout, and A.F.J. de Mulder, gravity and a model of the median valley, *J. Geophys., 47*, 91-98, 1980.

Gahagan, L. M., et al., Tectonic fabric map of the ocean basins from satellite altimetry data, *Tectonophysics, 155*, 1-26, 1988.

Hey, R. N., and D. S. Wilson, Propagating rift explanation for the tectonic evolution of the northeast Pacific—The pseudomovie, *Earth Planet. Sci. Lett., 58*, 167-188, 1982.

Haxby, W. F., and D.L. Turcotte, On isostatic geoid anomalies, *J. Geophys. Res., 83*, 5473-78, 1978.

Klitgord, K. D., and J. Mammerickx, Northern East Pacific Rise: Magnetic anomaly and bathymetric framework, *J. Geophys. Res., 87*, 6725-6750, 1982.

Klitgord, K.D., and J.D. Mudie, The Galapagos Spreading Center: A near bottom geophysical survey, *Geophys. J. R. Astron. Soc., 38*, 563-586, 1974.

Macdonald, K. C., Mid-ocean Ridges: Fine scale tectonic, volcanic, and hydrothermal processes within the plate boundary zone, *Annu. Rev. Earth Planet. Sci., 10*, 155-190, 1982.

Macdonald, K. C., The Crest of the Mid-Atlantic Ridge: Models for crustal generation processes and tectonics, *in The Geology of North America, vol. M, The Western North Atlantic Region, edited by P.R. Vogt and B.E. Tucholke,* Geological Society of America, Boulder, Colo., 1986.

Macdonald, K. C., and B.P. Luyendyk, Deep tow studies of the structure of the Mid-Atlantic Ridge crest near lat. 37°N, *Geol. Soc. Am. Bull., 88*, 621-636, 1977.

Marsh, J.G., and T.V. Martin, The Seasat altimeter mean sea surface model, *J. Geophys. Res., 87*, 3269-3280, 1982.

Menard, H. W., Seafloor spreading, topography and the second layer, *Science, 157*, 923-924, 1967.

Phipps Morgan, J., E.M. Parmentier, and J. Lin, Mechanisms for the origin of mid-ocean ridge axial topography: Implications for the thermal and mechanical structure of accreting plate boundaries, *J. Geophys. Res., 92*, 12,823-12,836, 1987.

Rea, D. K., Asymmetric seafloor spreading and a nontransform axis offset: the East Pacific Rise 20°S survey area.,*Geol. Soc. Am. Bull., 89*, 836-844, 1978.

Sleep, N.H., Sensitivity of heat flow and gravity to the mechanism of seafloor spreading, *J. Geophys. Res., 74*, 542-549, 1969.

Tapponier, P., and J. Francheteau, Necking of the lithosphere and the mechanics of slowly accreting plate boundaries, *J. Geophys. Res., 83*, 3955-3970, 1978.

Vogt, P. R., Plumes, subaxial pipe flow and topography along the mid-oceanic ridge, *Earth Planet. Sci. Lett., 29*, 309-325, 1976.

C. Small and D.T. Sandwell, Geological Research Division, Scripps Institution of Oceanography, La Jolla, CA 92093.

(Received August 16, 1988;
revised May 25, 1989;
accepted May 12, 1989)